40th AIAA Fluid Dynamics Conference, 28 June – 1 July 2010, Chicago, Illinois

DNS of transition in supersonic boundary layers

Suman Muppidi *& Krishnan Mahesh †
Aerospace Engineering & Mechanics
University of Minnesota

This paper performs Direct Numerical Simulation of transition induced by blowing and suction in a spatially evolving Mach 2.25 supersonic boundary layer. We use a novel algorithm (Park & Mahesh 2007) capable of solving compressible flow on unstructured grids. Our objective is to evaluate our unstructured capability to simulate supersonic transition. Transition is achieved using controlled periodic fluctuations over a region of the wall. It is observed that the applied perturbation produces streamwise vortices which breakdown to produce a turbulent boundary layer. The results of the turbulent region are compared to available data and a good agreement is obtained. The transition process is highly unsteady and localized, and the paper presents the sensitivity of the transition location to the streamwise mesh resolution.

I. Introduction

Predicting and understanding compressible high speed flows is essential for the development of high speed vehicles and engines. The flows are frequently turbulent or transitional, and exhibit high rates of heat transfer and skin friction in the boundary layer. The process of transition is very sensitive to disturbances, numerical errors, surface roughness and geometric imperfections, making reliable computations very challenging. Even as the flow becomes turbulent, it involves a wide range of scales of motion, and accurate computations are far from being straight–forward. Simulating practical high speed flows using RANS is computationally efficient, but may not be accurate enough for transitional flows. Large Eddy Simulations (LES) and Direct Numerical Simulations (DNS) are more accurate, but demand suitable numerical techniques and computational meshes, and come with a high computational cost. We are developing the DNS/LES capability to simulate transitional and turbulent flows on practical geometries. The focus of this paper is to use DNS to investigate the process of transition in a supersonic boundary layer.

Guo & Adams (1994) used quasi–periodic simulations to obtain turbulent boundary layer flows past a flat plate. Adams & Kleiser (1996) study the growth of disturbances on a flat plate at Mach 4.5 using a temporal approach. Guarini & Moser (2000) performed DNS of a supersonic boundary layer at Mach 2.5. It is assumed that the boundary layer grows slowly in the streamwise direction and, hence, can be treated as being approximately homogeneous in this direction. Martin (2007) demonstrates a cost-effective method of simulating turbulent supersonic boundary layers using the RANS solution of a supersonic flow, and the fluctuation data of a subsonic flow, when transformed suitably, gives rise to a realistic turbulent boundary layer. These methods to simulate turbulent flows involve making one or more assumptions on the flow – slow boundary layer growth, small compressibility effects, similarities with incompressible boundary layers etc. A fully spatial numerical simulation that does not make any such assumption is considerably more expensive to perform. Two such examples of recent studies have been by Gatski & Erlebacher (2002) and Pirozzoli, Grasso and Gatski (2004) both of who performed DNS of spatially evolving boundary layer past a flat plate at Mach 2.25. However, these studies focus on the fully turbulent flow, and not on the process/mechanism of transition that causes it. Rist & Fasel (1995) performed DNS of controlled transition in an incompressible boundary layer flow, and identified breakdown mechanisms. Mayer *et al.* (2007, 2008) study the transition

*Research associate, Aerospace Engineering & Mechanics, AIAA member
†Associate Professor, Aerospace Engineering & Mechanics, AIAA member

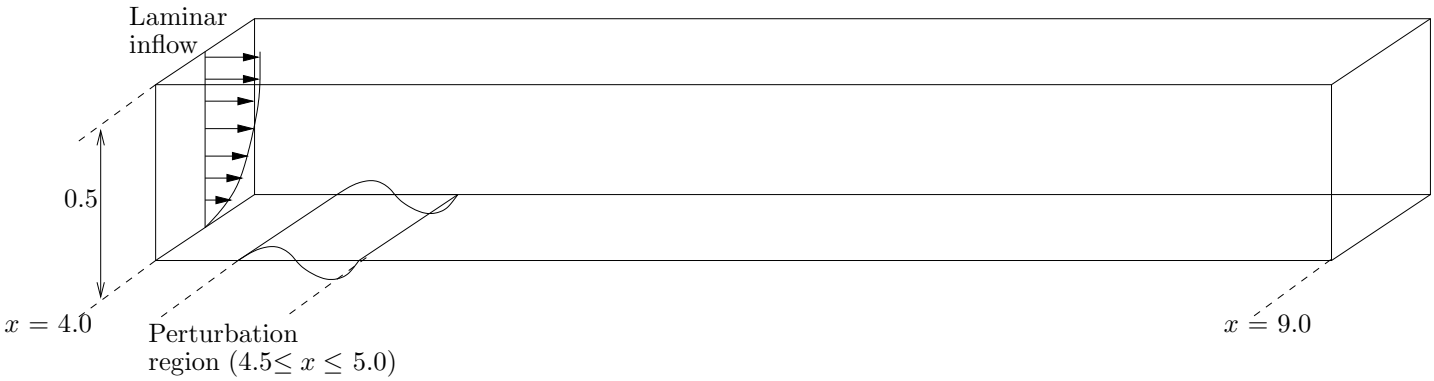

Figure 1. Schematic of the problem. The incoming laminar boundary layer thickness is $\delta \sim$ 0.0175.

in Mach 2 and Mach 3 laminar boundary layers initiated by a pair of oblique waves using DNS. They show that this oblique breakdown leads to a fully developed turbulent boundary layer.

The above work uses structured grids which are not easily applied to practical geometries. We are developing a DNS/LES solver for unstructured grids which can be readily applied to complex configurations. Our numerical method (Park & Mahesh 2007) has a base scheme that is non–dissipative and robust to enable simulations of broadband turbulent flows, and a corrector step that applies shock–capturing. The algorithm solves the compressible Navier–Stokes equations using a finite volume approach, and employs a modified least–squares approach to reconstruct the fluxes at cell faces (that makes the convective flux computation more accurate), and a scheme to split the viscous stress tensor into the compressible and the incompressible parts (that makes the viscous flux computation more accurate). A characteristic filter based shock capturing scheme provides stable solutions in the presence of discontinuities. The filter is designed to be active only in the vicinity of the shock, hence not adding any numerical dissipation in regions away from shocks (in the turbulent regions of the boundary layer, for example).

This algorithm is used to study the transition in a supersonic boundary layer at Mach 2.25. Transition is induced by periodic blowing and suction over a region of the wall. The purpose of the present paper is to evaluate our methodology for simulating high speed transition, discuss transition process, and the numerical issues involved. Section II presents the algorithm. The problem and computational setup are explained in section III. Validation of the turbulent region is presented in section IV A. Section IV B presents the flow as it transitions, and in section IV C, we present the sensitivity of this flow to grid refinement.

II. Numerical Details

We solve the compressible Navier–Stokes equations on unstructured grids. The governing equations are

$$\begin{aligned} \frac{\partial \rho}{\partial t} &= -\frac{\partial}{\partial x_k}\left(\rho u_k\right), \\ \frac{\partial \rho u_i}{\partial t} &= -\frac{\partial}{\partial x_k}\left(\rho u_i u_k + p\delta_{ik} - \sigma_{ik}\right), \\ \frac{\partial E_T}{\partial t} &= -\frac{\partial}{\partial x_k}\left\{\left(E_T + p\right) u_k - \sigma_{ik} u_i - Q_k\right\}, \end{aligned} \tag{1}$$

where ρ, u_i, p and E_T are density, velocity, pressure and total energy, respectively. The viscous stress σ_{ij} and heat flux Q_i are given by

$$\sigma_{ij} = \frac{\mu}{Re}\left(\frac{\partial u_i}{\partial x_j} + \frac{\partial u_j}{\partial x_i} - \frac{2}{3}\frac{\partial u_k}{\partial x_k}\delta_{ij}\right), \tag{2}$$

$$Q_i = \frac{\mu}{(\gamma-1)M_\infty^2 RePr}\frac{\partial T}{\partial x_i} \tag{3}$$

after non-dimensionalization, where Re, M_∞ and Pr denote the Reynolds number, Mach number and Prandtl number respectively.

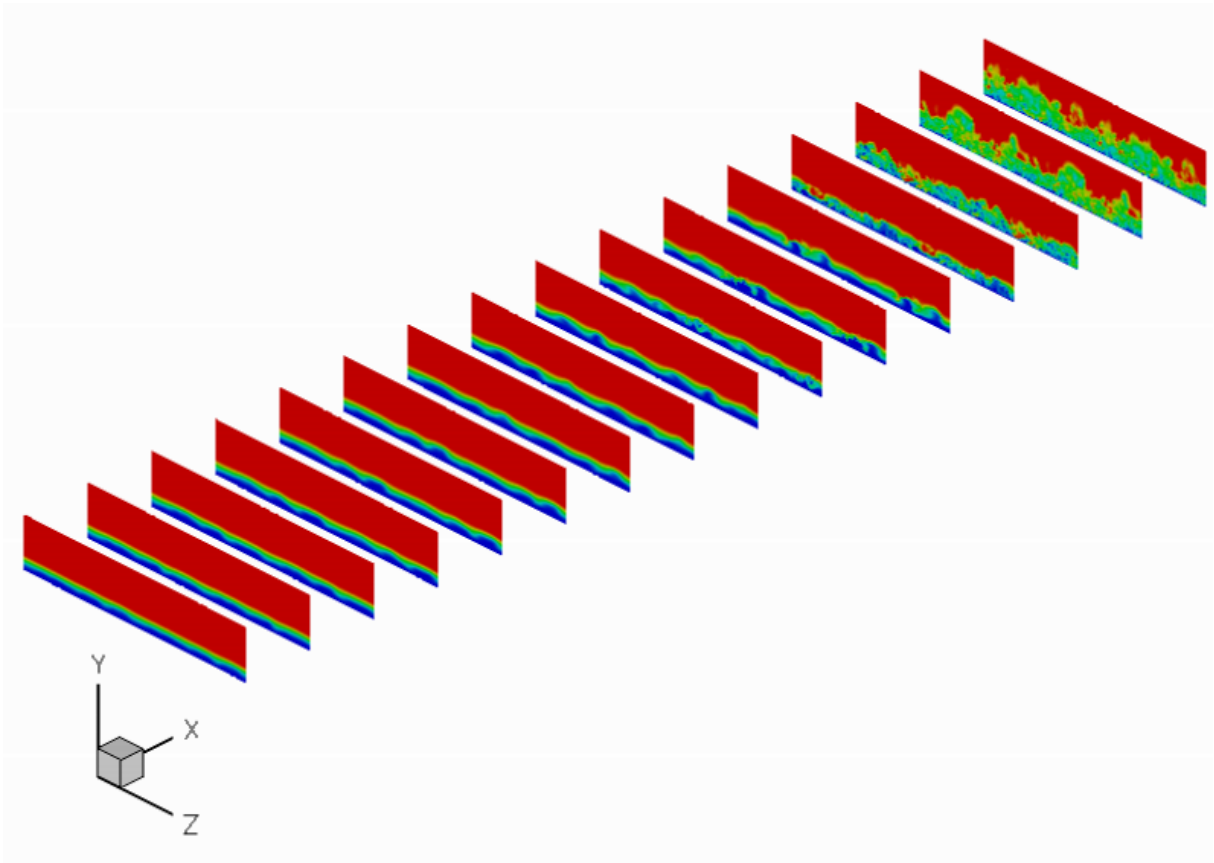

Figure 2. Spatial evolution of the flow using contours of density. The amplitude of the spanwise perturbations increases with downstream distance, giving rise to a three dimensional flow field, increased unsteadiness and eventually, turbulence. The domain is repeated once in the span.

The governing equations are discretized using a cell–centered finite volume scheme. Upon integration over the control volume, application of the Gauss theorem, and some rearrangement, the governing equations may be written as

$$\begin{aligned}
\frac{\partial \rho_{\mathrm{cv}}}{\partial t} &= -\frac{1}{V_{\mathrm{cv}}} \sum_{\text{faces}} \rho_f v_N A_f, \\
\frac{\partial \left(\rho u_i\right)_{\mathrm{cv}}}{\partial t} &= -\frac{1}{V_{\mathrm{cv}}} \sum_{\text{faces}} \left[\left(\rho u_i\right)_f v_N + p_f n_i - \sigma_{ik,f} n_k \right] A_f, \\
\frac{\partial \left(E_T\right)_{\mathrm{cv}}}{\partial t} &= -\frac{1}{V_{\mathrm{cv}}} \sum_{\text{faces}} \left[\left(E_T + p\right)_f v_N - \sigma_{ik,f} u_{i,f} n_k - Q_{k,f} n_k \right] A_f,
\end{aligned} \tag{4}$$

where V_{cv} is the volume of CV, A_f is the area of the face, n_i is the outward normal vector at surface, and v_N is the face-normal velocity. $\mathbf{q}_{\mathrm{cv}} = \left(\int_{\mathrm{cv}} \mathbf{q} dV\right) / V_{\mathrm{cv}}$ is the volume average within the cell, where $\mathbf{q} = (\rho, \rho u_i, E_T)$ is the vector of conservative variables. Here, the subscript f denotes interpolated values at each face of the control volume. Discretization of the governing equations involves reconstruction of the variables at the faces from the cell center values. Also, the spatial accuracy of the algorithm is sensitive to this flux reconstruction. The simulations employ a Modified least–square method (Park & Mahesh 2007) for this reconstruction, which can be shown to be more accurate than a simple symmetric reconstruction, and more stable than a least–square reconstruction. The algorithm uses a novel shock–capturing scheme that localizes numerical dissipation to the vicinity of flow discontinuities – thereby minimizing unnecessary

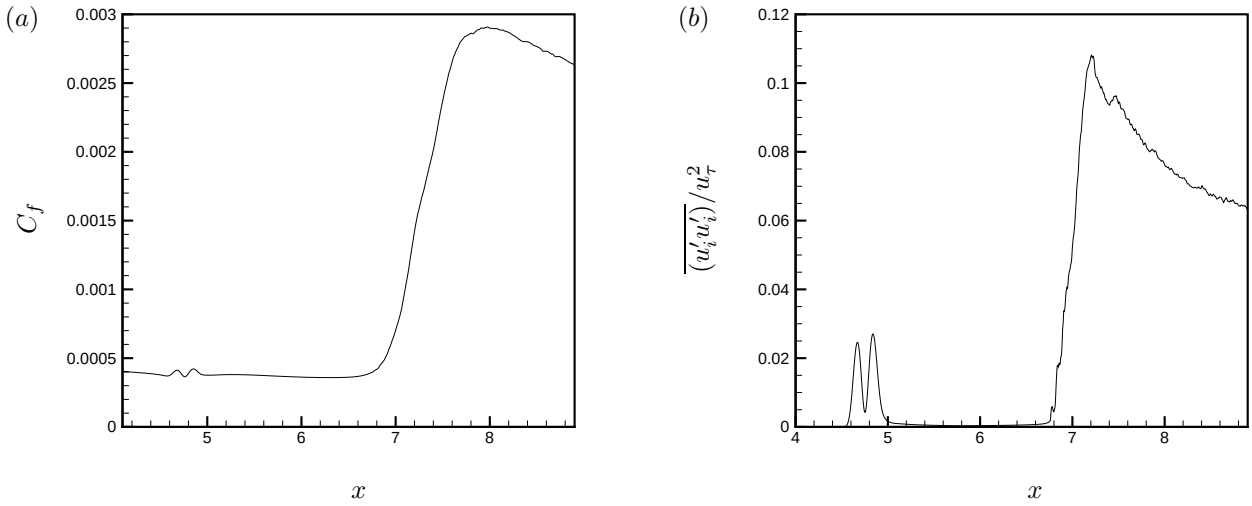

Figure 3. Variation of (a) skin friction coefficient and (b) turbulent kinetic energy along the wall.

dissipation. The solution is advanced in time using a second–order explicit Adams–Bashforth scheme, as

$$q_j^{n+1} = q_j^n + \frac{\Delta t}{2}\left[3\mathrm{rhs}_j(\mathbf{q}^n) - \mathrm{rhs}_j(\mathbf{q}^{n-1})\right], \tag{5}$$

where rhs_j denotes j th component of r.h.s. of Eq. (4), and superscript n denotes n th time step. The algorithm has been used to solve a variety of simple problems, as presented in Park & Mahesh (2007).

III. Simulation setup

The objective of the present simulations is to study the transition of a laminar flow past a flat plate at Mach 2.25 under periodic blowing and suction. A schematic of the computational domain is shown in figure 1. The domain extends from x = 4.0 to x = 9.0 length units (inches). The wall normal extent is 0.5 and the spanwise extent is 0.175. The unit Reynolds number is 635000 (per inch). Incoming flow is laminar, at Mach 2.25, with its origin at x = 0. Transition is induced by by prescribing a perturbation (wall–normal component) velocity at the wall, as prescribed by Pirozzoli *et al.* (2004):

$v = Au_\infty f(x)g(z)h(t)$

where

$f(x) = 4sin\theta\,(1 - cos\theta)\,/\sqrt{27}$

$\theta = 2\pi\,(x - x_a)\,/\,(x - x_b)$

$g(z) = \sum_{l=0}^{l_{max}} Z_l sin\,[2\pi l\,(z/z_{max} + \phi_l)]$, $\sum_{l=0}^{l_{max}} Z_l = 1.0$, and $Z_l = 1.25Z_{l+1}$

$h(t) = \sum_{m=1}^{m_{max}} T_m sin\,[2\pi\,(\beta t + \phi_m)]$, $\sum_{l=0}^{l_{max}} T_m = 1.0$, and $T_m = 1.25T_{m+1}$

Only the flow between $x = 4.5$ and $x = 5.0$ is perturbed. $x_a = 4.5$ and $x_b = 5.0$. A is the amplitude of the perturbation and is $0.04u_\infty$, β is the temporal frequency (taken to be 75 KHz), and ϕ_l and ϕ_m are random phases ($0 \le \phi_l, \phi_m \le 1$). From these expressions, it can be seen that the perturbation velocity is periodic and varies in x and z, as well as in time. Also, the perturbation velocity is always zero at x_a and x_b. The dimensional temporal frequency of the perturbation, 75 KHz gives a time period (T_{pert}) of 1.333×10^{-5}. If sonic speed is assumed to be about 350 m/s and the reference length L_r taken to be 1 inch, the convective

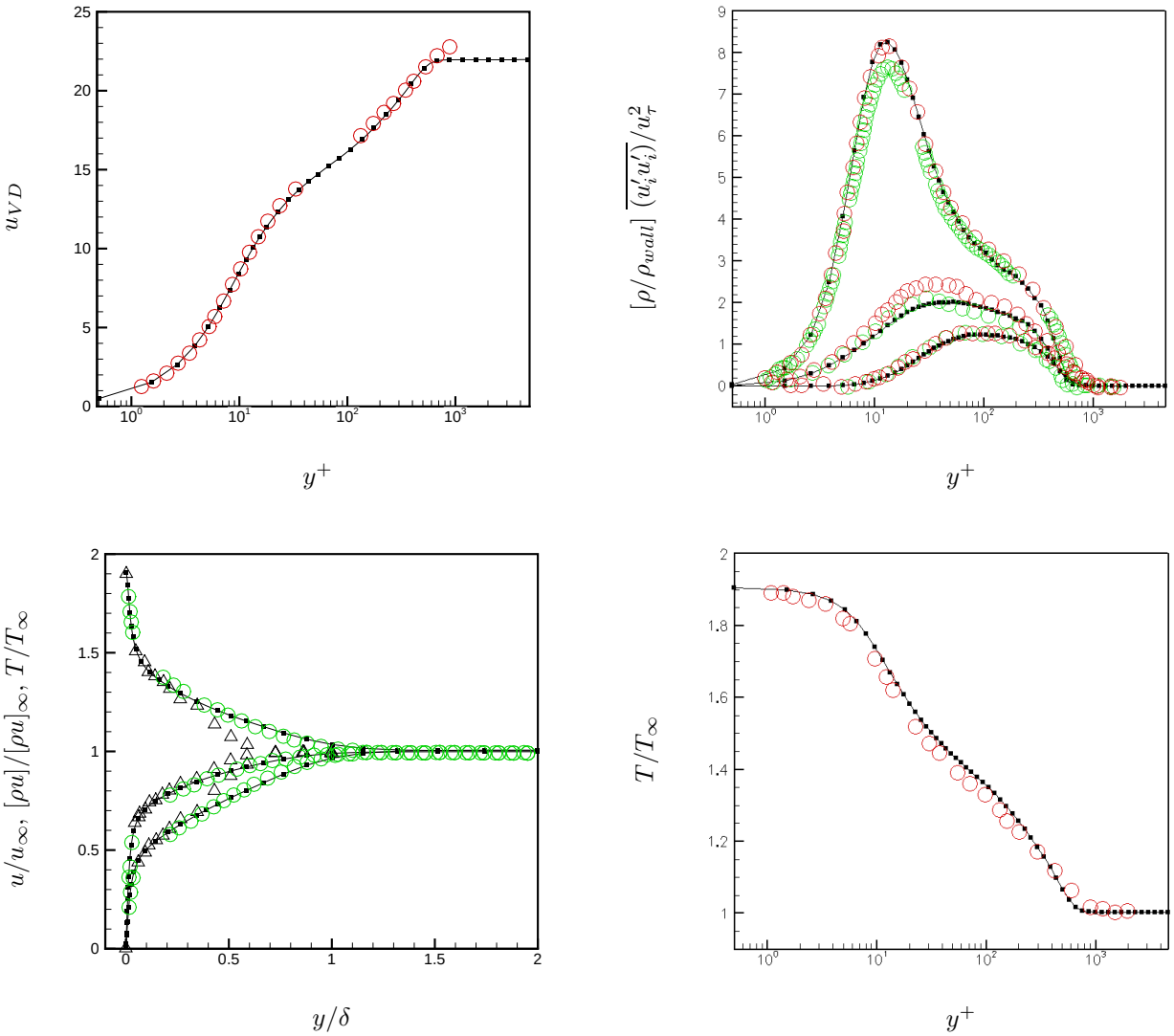

Figure 4. Comparison of present simulation with available results. Lines: simulation, red circles: Gatski & Erlebacher simulation, green circles: Pirozzoli *et al.* simulation, triangles: Shutts *et al.* experiment.

time scale based on u_∞ and L_r is: $T_r = L_r/u_\infty \sim 3.2 \times 10^{-5}$, that is, of the same order of magnitude as T_{pert}.

The solution to the compressible Blasius flow is prescribed at the inflow. Periodic boundary conditions are prescribed at the spanwise boundaries. At the wall, isothermal boundary conditions are used for temperature, and a zero–gradient condition is used for pressure. These boundary conditions apply even over the perturbation region. Zero gradient boundary conditions are used at the outflow. At the top boundary, freestream conditions are specified for u, p, T and ρ. A zero normal–derivative condition is imposed on v and w. Sutherland's formula is used to compute viscosity. Computations are performed over a mesh consisting of 2400 control volumes in the streamwise direction, 56 in the wall–normal direction and 192 in the spanwise direction. The mesh spacing is non–uniform in the wall–normal direction, such that the elements closest to the wall are the finest. The mesh sizes are: $\Delta x = 0.002$, $\Delta y_{min} = 5 \times 10^{-5}$, and $\Delta z = 9 \times 10^{-4}$.

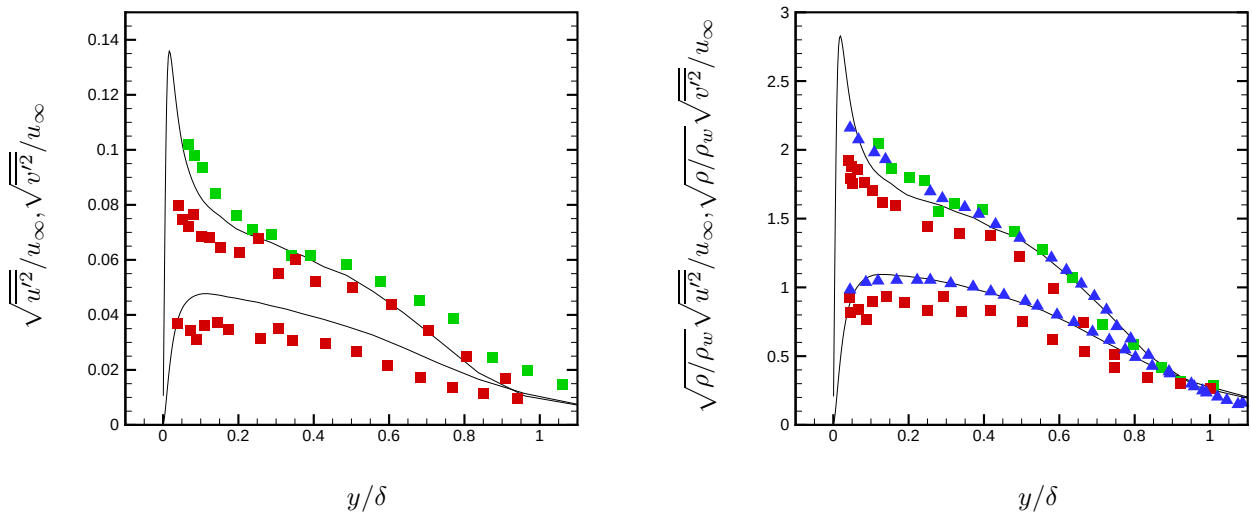

Figure 5. Comparison of turbulent intensity profiles ($\overline{u_i'u_i'}$ and $\overline{v_i'v_i'}$) with experiment. Triangles are data from Klebanoff; Squares are data from Elena *et al.* (red: two component LDV, green: one component LDV). Lines are profiles from the present simulation.

IV. Results

Figure 2 presents an instantaneous snapshot of the flow. The x and y axes denote the streamwise and wall–normal directions respectively, and z denotes the span. Close to the inflow, the wall–normal perturbations cause spanwise variation in the boundary layer profile. The amplitude of these perturbations appears to increase with downstream distance, and the velocity field appears to be three dimensional. Further downstream, the boundary layer appears to transition and give rise to a turbulent flow. Note that the present simulation makes no simplifying assumptions about the flow, and solves for the natural spatial evolution of the boundary layer under the influence of the forcing at the wall.

This section presents details of the flow field as it evolves along the computational domain. Section IV A uses the time–averaged statistics of the flow and validates it against available simulation and experimental data. Section IV B discusses the transition process, and presents the flow field between the laminar and turbulent regions. In section IV C, the dependence of the results on computational mesh is discussed. While the importance of adequate wall–normal and spanwise resolution for turbulent boundary layer flows is well known, our simulations show that the transitional flow is also sensitive to the mesh resolution in the streamwise direction.

A. Turbulent region

Figure 3 shows the variation of the skin friction coefficient C_f and the turbulent kinetic energy $\overline{(u_i'u_i')}$ along the length of the wall, starting from the inflow ($x = 4.0$). Both these curves indicate the perturbation region ($4.5 \leq x \leq 5.0$). Upstream of the perturbation region, the flow is laminar. To some extent downstream of the perturbation region, both C_f and $\overline{(u_i'u_i')}$ curves exhibit laminar behavior. There is an increase in the values of the skin friction coefficient and the turbulent kinetic energy beginning at about $x = 6.5$. The curves reach a peak at about $x = 7.0$ and gradually decrease further downstream. This suggests that the flow begins to transition only past $x = 6.0$ and that the region downstream of $x = 7.5$ may be considered to be turbulent.

The time averaged profiles from the present simulation are compared to available data in figure 4. The Van Driest transformed velocity u_{VD} at $x = 8.75$ is compared to the profile from the simulation of Gatski & Erlebacher (2002). The comparison is reasonable. We also compare velocity intensities normalized with the wall density ($[\rho/\rho_{wall}]\overline{(u_i'u_i')}/u_\tau^2$ etc) to similar profiles from Gatski & Erlebacher and Pirozzoli *et al.* (2004). Figure also shows streamwise velocity u/u_∞, momentum $[\rho u]/[\rho u]_\infty$ and temperature t/T_∞ profiles plotted against the wall normal distance normalized with the boundary layer thickness (δ is the location 99% of the freestream velocity). The experimental data on this curve is from Shutts *et al.* (1955). Similar

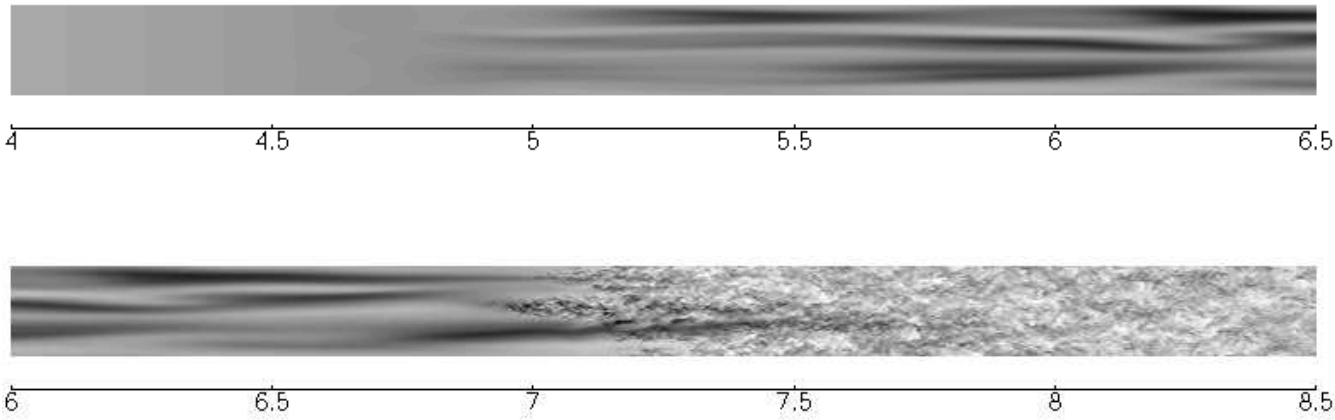

Figure 6. Horizontal slices close to the wall show the spatial evolution of the flow. Periodic perturbation produces streamwise streaks which breakdown and cause the flow to transition.

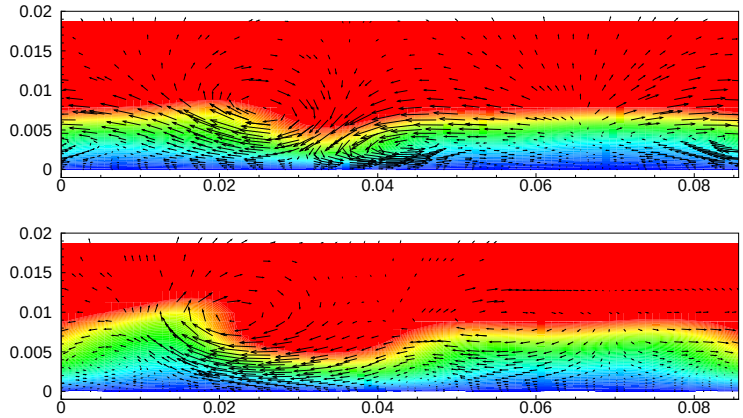

Figure 7. A snapshot of the end–view through the streaks, at $x = 5.0$ and $x = 6.0$. Picture shows only a part of the domain. In–plane velocity vectors show the presence of streamwise vortices.

profiles from Pirozzoli *et al.* are also shown. As observed by them, the experimental profiles show a bump in the profiles of velocity and temperature in the vicinity of $y/\delta = 0.5$, which is not observed in profiles from their simulations, or ours. The last plot compares the profile of temperature (against y^+) with that from simulations of Gatski & Erlebacher. Once again, reasonable agreement is observed. Note that the thermal boundary condition at the wall is isothermal, with T_{wall} set to be the adiabatic temperature at Mach 2.25. The gradient at the wall is very close to zero indicating minimal, if any, heat transfer at the wall.

Figure 5 presents a few more comparisons with experimental data. Elena *et al.* (1985) perform Laser Doppler Velocimetry (LDV) and hot–wire anemometry measurements in a supersonic turbulent boundary layer at Mach 2.32 and a Reynolds number of 67100 (based on the boundary layer thickness of the turbulent boundary layer at the measurement location). The focus of their paper is to compare different measurement techniques. They use their data to show that results obtained using one–component LDV differ significantly from two–component LDV results, and that the one–component LDV results provide a better agreement with the experimental data of Klebanoff (1955), which is also included in figure 5. Klebanoff's data corresponds to the hot wire measurements of a zero–pressure gradient boundary layer and the measurement location corresponds to a Re_x of 4.2 $\times 10^6$. Profiles of turbulent intensity from the present simulation non–dimensionalized with u_∞ are compared to the data from Elena *et al.* while the density weighted intensities are also compared with Klebanoff data. We have a good agreement with the one–component LDV results of Elena *et al.* and the hot wire measurements of Klebanoff. While the snapshot from the simulation (figure

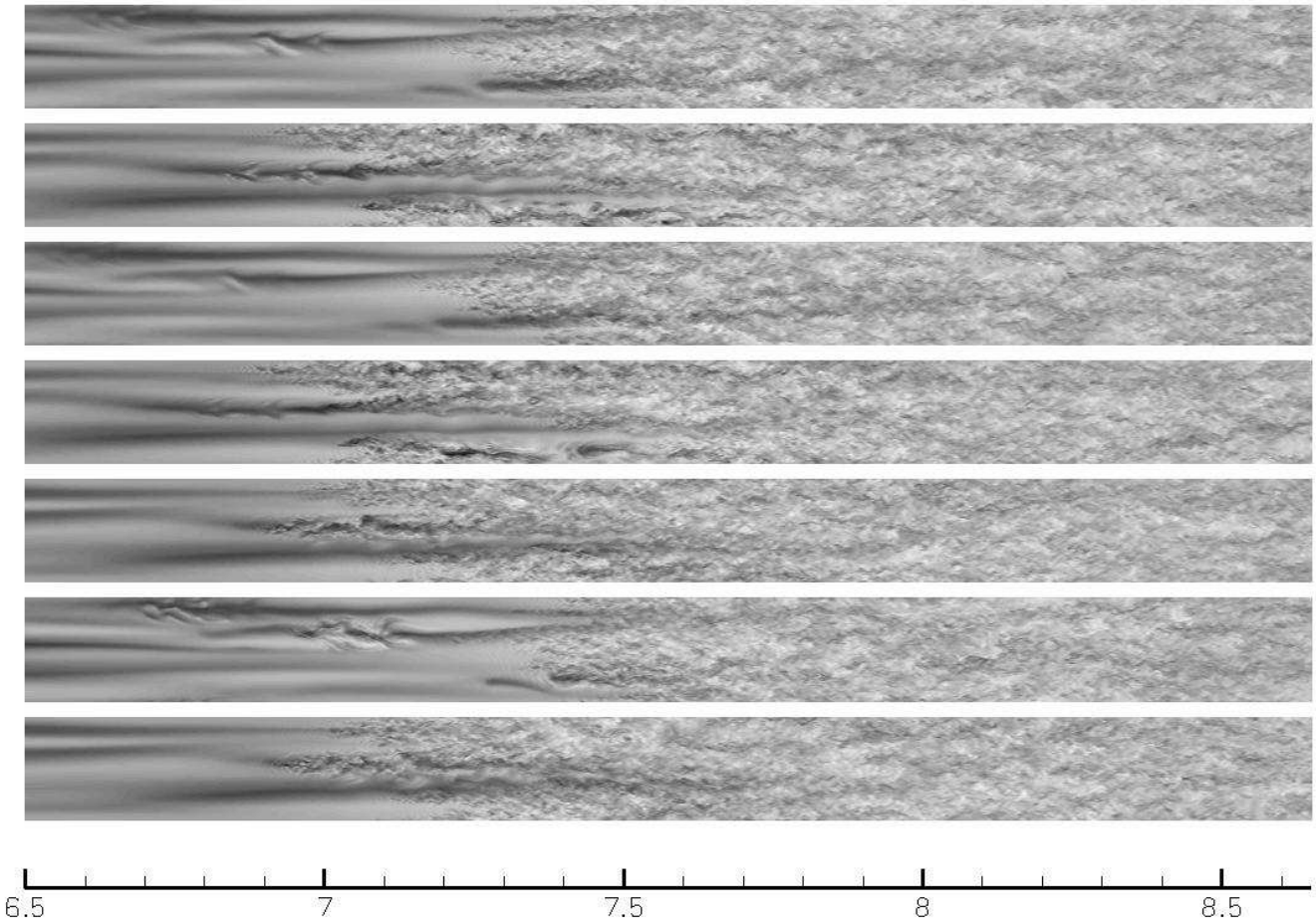

Figure 8. Snapshots of the flow using contours of streamwise velocity on the plane $y = 0.01$ at various instants of time. Evolution in time is shown moving bottom to top.

2) gives visual evidence of transition to turbulence, the comparison and validation in figures 4 and 5 show that the flow is indeed turbulent and fully developed.

B. Flow transition

Figure 6 shows the contours of streamwise velocity on a plane parallel to the wall and close to it ($y = 0.01$). The length of the domain is broken into the two pictures, and the contour levels adjusted, to show the flow features in greater detail. The top figure shows the flow in the region ($4.0 \leq x \leq 6.5$) to be laminar, as is borne out by the skin friction curve in figure 3. The figure shows the long streamwise streaks resulting from the perturbation at the wall ($4.5 \leq x \leq 5.0$). The bottom figure shows a portion of these streaks and the subsequent turbulent region. At this instant, the onset of turbulence appears to be around $x \sim 7.0$. From figure 3, this corresponds to the location where the skin friction value begins to rise from the laminar value. Visually, it appears that it is the breakdown of these streaks that causes the flow to transition.

In order to observe the make up of these streaks, figure 7 presents a couple end–view snapshots. Shown are the contours of streamwise velocity at two streamwise locations ($x = 5$ and $x = 6$), along with a few representative vectors that show the in–plane velocity field. The contours show the spanwise perturbation of the boundary layer, and the vectors clearly show the presence of coherent streamwise vortices. Figure 6 shows the periodic change in the magnitude of the streaks (along x) and this can be explained by the fact that the perturbation velocity is a periodic function in time. As the perturbation velocity changes sign, vortices of opposite rotation are produced in the streamwise direction. While the vorticity direction at the

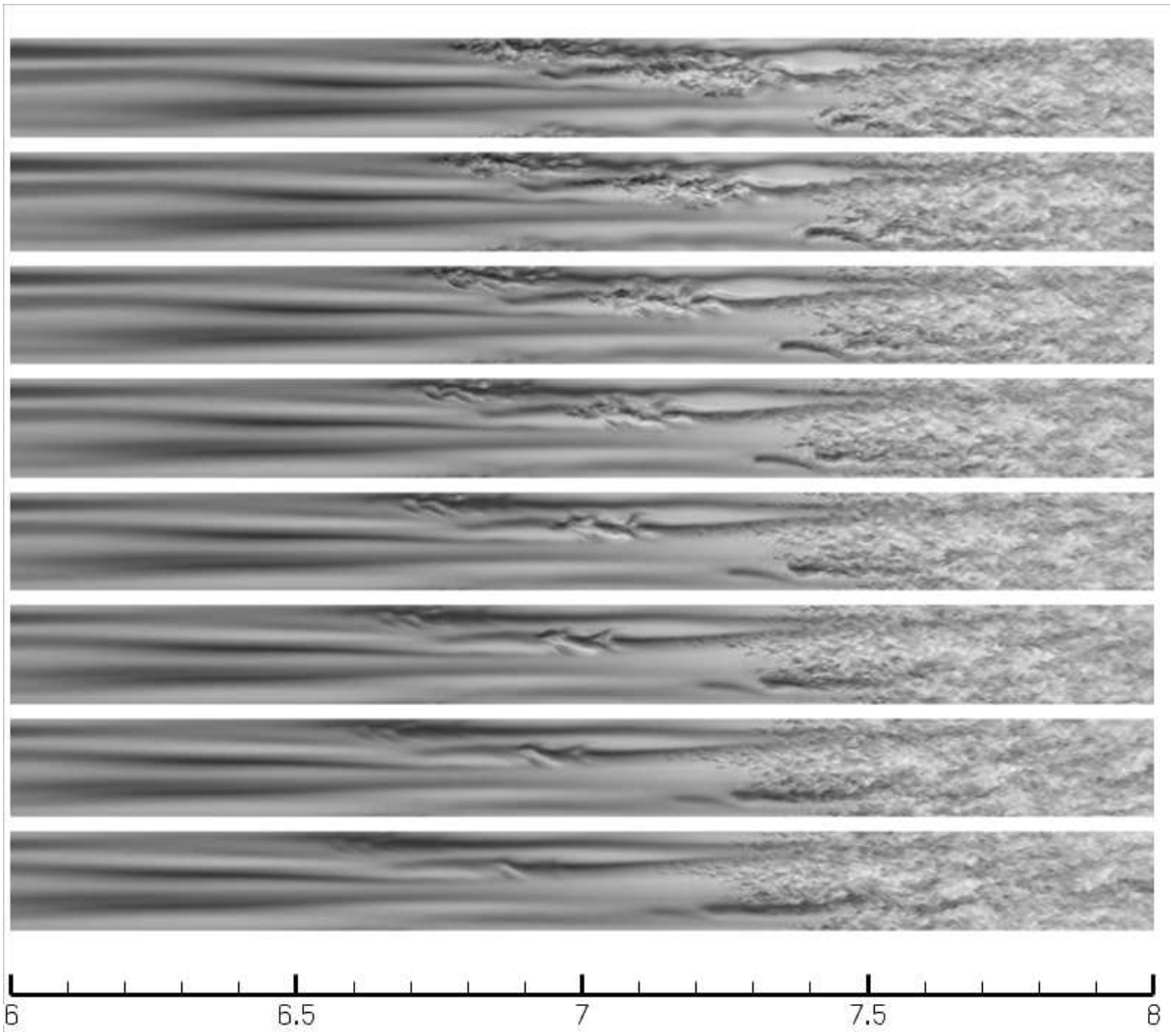

Figure 9. Snapshots of the flow separated by a small time interval, using contours of streamwise velocity on the plane $y = 0.01$. Temporal evolution is bottom to top, and shows a breakdown event as a streamwise vortex breaks down and later collapses into the turbulent front downstream.

two locations in figure 7 is the same, note that their spanwise location z is slightly different. This can also be gathered from the 'waviness' seen in figure 6.

Figure 8 shows the contours of streamwise velocity on a horizontal plane ($y = 0.01$, same as in figure 6) at different instants, roughly separated by the same interval. At all instants, the streamwise vortices are observed in the upstream part of the domain. The location of transition oscillates over a significant extent along x (note that one unit of length shown along the streamwise direction corresponds to just under 60 times δ_{inflow}). Note that in all these images, the flow at x=7.0 is mostly laminar while at x=8.0, it is always turbulent. This can be reconciled with figure 3 which showed the C_f curve to just begin rising at x=7.0, to peak before x=7.5 and to possess a negative slope by x=8.0. Figure 8 shows the process of transition to be highly unsteady and localized, and this inherent unsteady behavior renders reliable simulation of transition flows, and prediction of transition location, difficult.

A couple of instants in figure 8 show that the streamwise vortex breaks down upstream of the turbulent front. This can be seen as a 'kink' in the topmost figure at $x \sim 6.9$. In fact, the simulation results show periodic occurrence of these breakdown events. Figure 9 follows one such breakdown event, the temporal evolution being from bottom to top, and the images are separated by a small time interval. The sequence of images shows the break up of a streamwise vortex, increasing three–dimensionality and unsteadiness, and an eventual collapse (or absorption) into the turbulent front.

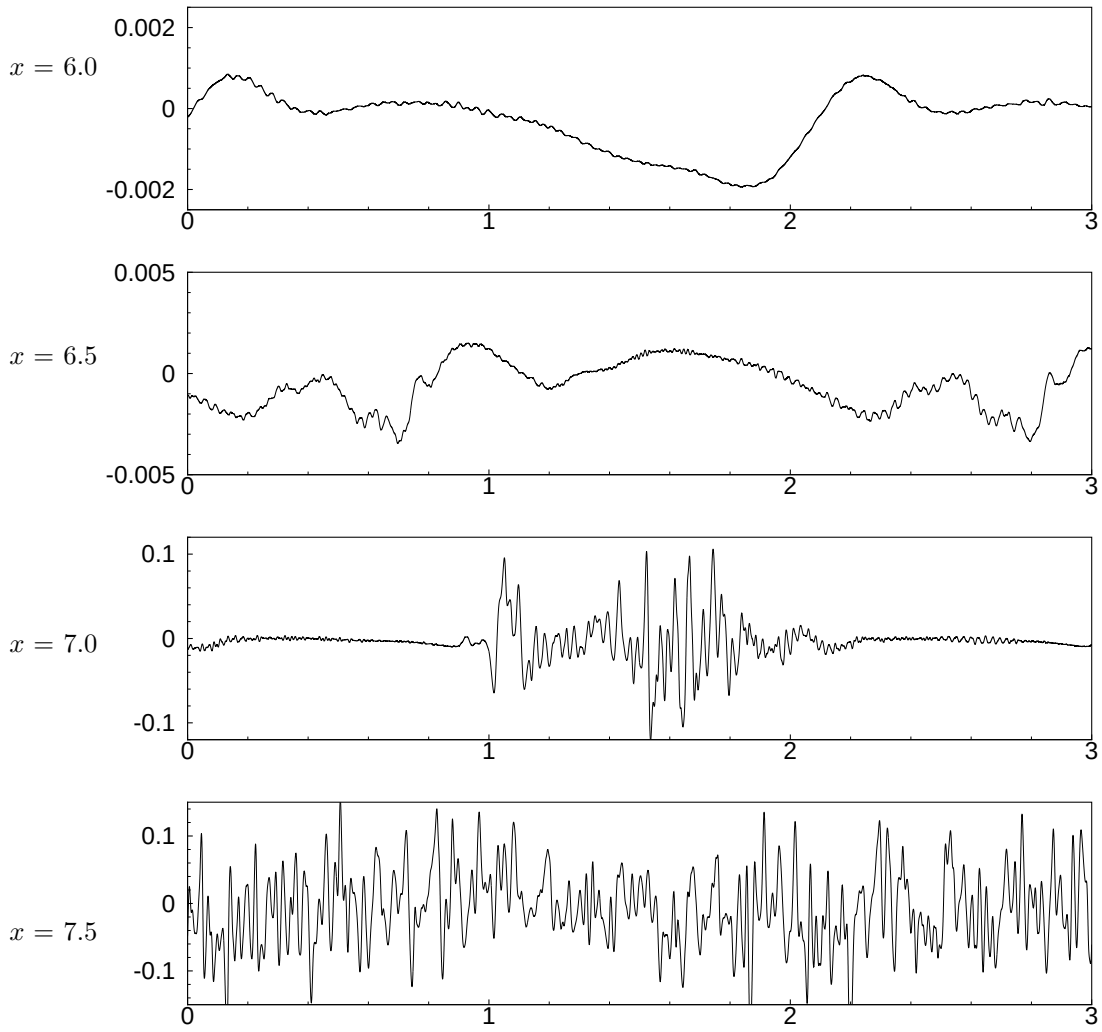

Figure 10. Time signal of wall–normal velocity at different streamwise locations: $x = 6.0$, 6.5, 7.0 and 7.5. All the signals correspond to $y = 0.01$, and the three–quarter span location $z = 0.0875$. The intermittent unsteady behavior at $x = 7.0$ corresponds to the vortex breakdown in figure 9.

The inherent unsteadiness in the flow, and the intermittency of the turbulent front are also apparent from figure 10. Figure shows the variation of wall–normal velocity v in time at four points at the same wall–normal and spanwise location ($y = 0.01$, $z = 0.0875$) and at different streamwise locations ($x = 6.0$, 6.5, 7.0 and 7.5). With increasing x, note that the amplitude of velocity fluctuation increases. The signal appears comprised of (comparatively) lower frequencies at $x = 6.0$ and exhibits a broadband turbulent behavior by $x = 7.5$. It is interesting to note how the signal at $x = 7.0$ shows a localized patch of unsteadiness; this corresponds to the intermittent vortex breakdown shown in figure 9.

C. Numerical Issues

Transition to turbulence in supersonic flows is inherently complex. Physically, it depends not only on the Reynolds number and the boundary layer thickness (which chiefly determine the flow field in an incompressible flow) but also on the Mach number, wall temperature, and thermal boundary conditions, to name a few. The flow field is highly unsteady and three dimensional. This is true not only of the forcing, the streamwise vortices and the turbulent flow but also of the transition location and the occasional breakdown of individual vortices. All these features place certain demands on the numerical techniques and tools used, to be able to accurately model and predict this flow.

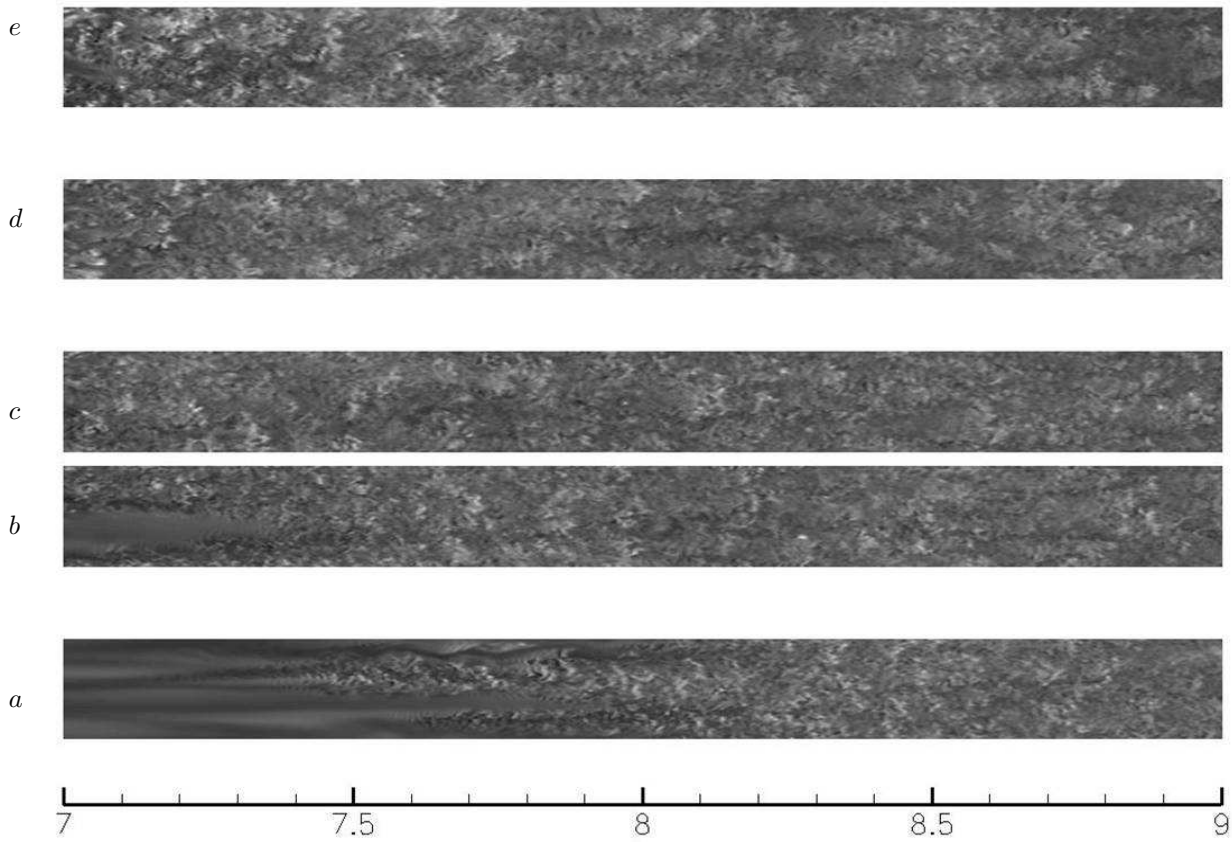

Figure 11. Snapshots from simulations on various grids. All of them have the same mesh resolution in the region $7.0 \leq x \leq 9.0$ but different Δx upstream. Figure 12 shows snapshots of the upstream region. Note that the flow in the turbulent region of the domain looks very reasonable.

The solution is sensitive to grid resolution. Insufficient wall–normal resolution leads to an incorrect peak location for the velocity intensity profile, for example. Comparing statistics of the solution using 96 elements in the spanwise direction, to the solution using 192 ($\Delta x, \Delta y$ being the same) did not change the location of transition but the values of skin friction and u_τ (C_f increased with grid refinement). The importance of wall–normal and spanwise resolution for turbulent simulations is well known. The present simulations indicate that the streamwise resolution is also important for simulation of flow transition. This is true not only of the turbulent flow region, but also in the laminar region upstream. Simulations were performed on grids with the same Δx between $x = 7$ and $x = 9$. The mesh was coarsened in the region x= 4.0 to $x = 7.0$. It was observed that while the flow appeared turbulent and believable in the turbulent region, the coarse grids caused the transition location to move farther upstream. Figure 11 shows only the turbulent region of the domain from all these simulations. Δx_{inflow} denotes the streamwise mesh spacing near the inflow and Δx_{turb} denotes the mesh spacing in the region between x=7.0 and $x = 9.0$. (a) shows the solution from a grid where Δx is the same throughout the domain. (b) and (c) show the solution at different instants of time from a simulation on a computational mesh where $\Delta x_{inflow} = 2.5\ \Delta x_{turb}$. Note that the mesh was exactly the same in y and z directions. (d) and (e) denote snapshots from simulations where Δx_{inflow} is 5.0 and 10.0 times Δx_{turb} respectively. Visually, all the solutions look reasonable, unsteady and turbulent. The difference in the solution can be observed in figure 12 which includes the coarse mesh part of the domain. Note that the transition location and the flow field leading to the transition are inaccurate for the coarser meshes. In fact, both (d) and (e) cause the flow transition to occur all over the domain, even upstream of the perturbation region (further in time than the snapshot shown in figure 12). Clearly, the transition location is inaccurate at coarse streamwise resolutions.

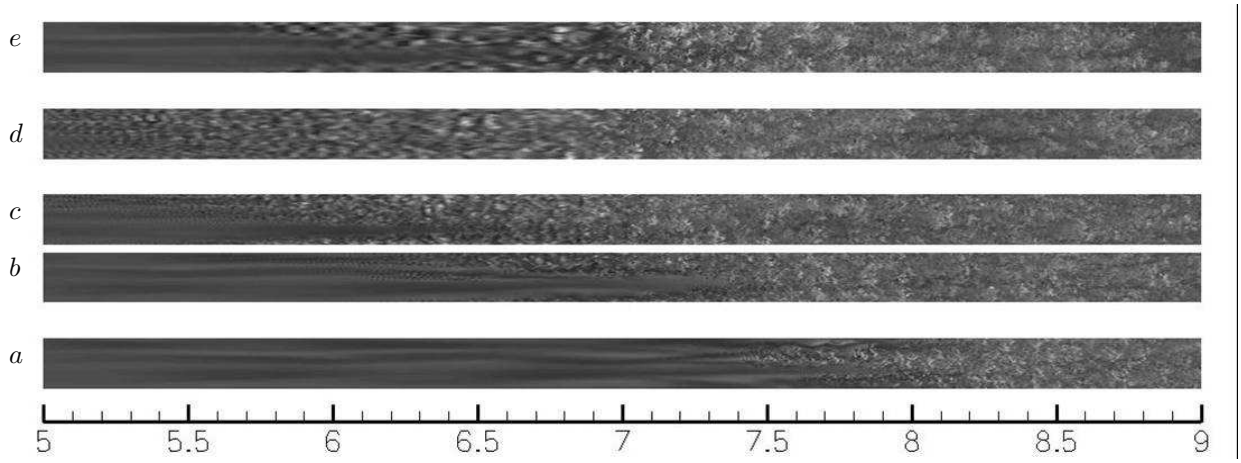

Figure 12. Snapshots from simulations on various grids. Figure follows figure 11. (a): Δx is the same everywhere, (b),(c): $\Delta x_{inflow} = 2.5\ \Delta x_{turb}$, (d): $\Delta x_{inflow} = 5.0\ \Delta x_{turb}$, and (e): $\Delta x_{inflow} = 10.0\ \Delta x_{turb}$. While the solution from all these computational grids looks reasonable in the turbulent region, insufficient resolution in the laminar region results in inaccurate transition behavior.

V. Acknowledgments

This work is supported by NASA under the hypersonics NRA program and by the Air Force Office of Scientific Research under contract FA9550-04-1-0341. Computer time for the simulations was provided by the Minnesota Supercomputing Institute (MSI), and Texas Advanced Computing Center through TeraGrid allocation.

References

[1]Adams, N. A. & Kleiser, L. 1996 Subharmonic transition to turbulence in a flat–plate boundary layer at Mach number 4.5, *J. Fluid Mech.* **317**.

[2]Elena, M., Lacharme, J. & Gaviglio, J. 1985 Comparison of hot-wire and laser Doppler anemometry methods in supersonic turbulent boundary layers. In *Proc. Intl Symp. on Laser Anemometry* (ed. A. Dybb & P. A. Pfund). ASME.

[3]Gatski, T. B. & Erlebacher, G. 2002 Numerical simulation of a spatially evolving supersonic turbulent boundary layer, *NASA Tech. Memo*–211934.

[4]Guarini, S. E, Moser, R. D, Shariff, K & Wray, A. 2000 Direct nimerical simulation of a supersonic turbulent boundary layer at Mach 2.5, *J. Fluid Mech.* **414**.

[5]Guo, Y. & Adams, N. A. 1994 Numerical investigation of supersonic turbulent boundary layers with high wall temperature, *proceedings of the summer program of the Center for Turbulence Research, Stanford University.*

[6]Klebanoff, P. 1955 Characteristics of turbulence in a boundary layer with zero pressure gradient, *NASA Rep.* 1247.

[7]Martin, P. 2007 Direct numerical simulation of hypersonic turbulent boundary layers. Part 1. Initialization and comparison with experiments, *J. Fluid Mech.* **570**.

[8]Mayer, C. S. J., Wernz, S. & Fasel, H. F. 2007 Investigation of Oblique Breakdown in a Supersonic Boundary Layer at Mach 2 using DNS, *AIAA Paper* 2007–949

[9]Mayer, C. S. J., von Terzi, D. A. & Fasel, H. F. 2008 DNS of Complete Transition to Turbulence Via Oblique Breakdwon at Mach 3, *AIAA Paper* 2008–4398.

[10]Park, N. & Mahesh, K. 2007 Numerical and modeling issues in LES of compressible turbulent flows on unstructured grids, *AIAA Paper* 2007–722.

[11]Pirozzoli, S., Grasso, F. & Gatski, T. B. 2004 Direct numerical simulation and analysis of a spatially evolving supersonic turbulent boundary layer at M=2.25, *Phys. Fluids* **16**.

[12]Rist, U. & Fasel, H. 1995 Direct numerical simulation of controlled transition in a flat-plate boundary layer, *J. Fluid Mech.* **298**.

[13]Shutts, W.H., Hartwig, W.H. and Weiler, J.E. 1955 Final Report On Turbulent Boundary Layer And Skin Friction Measurements on a Smooth, Thermally Insulated Flat Plate at Supersonic Speeds, University of Texas, Defense Research Laboratory Report 364.